An Isotropic Hopping Model for Singly Charged Xe Clusters

Demosthenes C. Athanasopoulos*

Department of Chemistry and Physical Sciences, Pace University, New York, New York 10038

Kevin E. Schmidt

Department of Physics and Astronomy, Arizona State University, Tempe, Arizona 85287

Received: November 13, 1997; In Final Form: November 13, 1997

This work introduces a theoretical model for the description of charged xenon clusters. It is based on the assumption that the charge migrates inside the cluster by isotropic hopping through a Hubbard Hamiltonian and treats Xe atoms as classical polarizable particles. For their interaction we use a 2-body potential to which we add charge−charge, charge−dipole, and dipole−dipole interactions. The calculations are carried out within the ground state approximation. We are primarily concerned with the following issues: (1) the role that the quantum degree of freedom plays on the magic number pattern, and (2) the question of dimer formation inside the clusters. To investigate these questions we perform simulated annealing and molecular dynamics calculations on neutral and singly-charged clusters of up to 25 atoms. Our results confirm that the magic number pattern is related to the geometric structure of the clusters, as previously published (*Surf. Sci.* **1985**, *156*, 370). Further, we demonstrate that the magic number pattern is not affected by the electrostatic interactions or the quantum effect on the charge distribution of the electric charge. Our model does not result in any dimer formation. We calculate the binding energies and the adiabatic ionization potential and find that they are very close to the experimental values.

I. Introduction

Microclusters, which inhabit a state somewhere between that of gas and condensed matter, are especially useful for increasing our understanding of the nucleation process from a microscopic point of view. In particular, rare gas clusters have proven particularly amenable to both theoretical and experimental study because their valence electron shell is closed and their interactions are well represented by simple 2- and 3-body potentials.[2,3] This latter property allows efficient computer simulations of these systems, the results of which can be readily compared to available experimental results.[4−8] At the same time, however, the theoretical discussion of exactly what the experimental results measure is complicated by the fact that experiments measure clusters' stability using mass spectroscopy in which the neutral clusters are ionized.

In typical experiments, clusters of many different sizes are produced. The size of clusters is usually expressed in terms of the cluster number. This is the number of bonded atoms in a cluster. In analysis, there are distinct peaks in the mass spectroscopy for some cluster sizes. The number of atoms in these particularly stable clusters is called *magic number*.

In this work we present a theoretical model for charged xenon clusters for the purpose of exploring the significance of quantum effects in dynamic studies of charged clusters. Further, we test how appropriate the Hubbard Hamiltonian is for these physical systems. Thus, we model these clusters as classical aggregates consisting of polarizable Xe atoms which interact through a 2-body potential, and a positively charged quantum hole that hops between the Xe atoms according to a Hubbard Hamiltonian.[9] The motion of the charge is about 2 orders of magnitude faster than the motion of the nuclei. This model, therefore, makes it possible to distinguish and explore quantum effects apart from classical ones.

Theoretical research on clusters has focused mainly on understanding two issues. The first issue is the understanding of the magic numbers (in terms of the interatomic potential and geometrical structure of these clusters). The second related issue is the effect of ionization on the abundance of clusters of various sizes. Finally, theoretical studies ask, are the magic numbers for neutral and ionized clusters different? The magic number pattern can be interpreted by assuming that the clusters have icosahedral geometry[1] (see Figures 4, 5 and 6). With one exception, the sublimation energy calculated with these structures possesses maxima for clusters containing magic numbers of atoms of Xe,[10] preionized Ar,[11] or Ba.[12] The only discrepancy is for the magic number 25; according to the icosahedral geometry closed shells, a cluster with 26 atoms should be more stable. Conversely, this approach does not correctly predict the numbers for Ar (ionized after the formation of the cluster) and Kr.[13]

The effect of ionization on the stability of the clusters is associated with the migration of the charge inside the cluster and its final localization. Almost all of the theoretical efforts to understand the dynamics of charged clusters depend on the assumption that, for a short period of time after ionization occurs, the charge, through its migration, is trapped between two atoms because of the polarization field that it causes. That is to say, a dimer forms. This idea is supported by both experimental and theoretical studies of rare gas solids. The formation of this dimer explains the difference between the drift mobility of electrons and holes inside these solids.[14−17] The potential well of the charged rare gas dimers is very deep, and

S1089-5639(97)02960-5 CCC: $15.00
Published on Web 02/05/1998

therefore a considerable amount of energy is released during their formation. The relaxation of this binding energy will increase the kinetic energy of the rest of the atoms inside the clusters, and some of them will evaporate. In such cases the experimentally-observed magic numbers represent the relative stability only of the charged clusters. They do not provide any information about the stability of the corresponding neutral clusters. On the other hand, the formation of the dimer would cause dislocations in the structure of the cluster. Taking these dislocations into account, we cannot necessarily associate the observed magic numbers with the closed shells of the icosahedral geometry. Molecular dynamics calculations have been presented by other authors in the past.[4−8] In general, these calculations have used a Lennard-Jones 6-12 potential for the neutral atom interactions and an explicit calculation of the charge−dipole and dipole−dipole interactions. They presume that a dimer is formed, and include in their classical Hamiltonians an appropriate intramolecular potential for the atoms that constitute the dimer. The charge migration was taken into account explicitly in one publication[7] by using Monte Carlo equilibration steps for the location of the dimer between successive molecular dynamics steps.

Our approach to this problem is to find, without making a previous assumption, how the charge is localized inside the cluster. We start with the same assumptions for the classical part as the previous authors (the 2-body potential and the point-polarizability model), and we attempt to study dimer formation by explicitly incorporating the charge migration in our calculations. We perform molecular dynamics and simulated-annealing calculations on small, positively charged xenon clusters. In our results we find no evidence of any dimer formation. However, we are able to calculate the binding energies of these clusters and to derive from these results the adiabatic ionization potentials, which are very close to the experimental values.[18,19] We also calculate the sublimation energy for clusters of up to 23 atoms, and we concur with earlier findings that the magic numbers 13 and 19 correspond to clusters with icosahedral geometry for which the sublimation energy gets its maximum values.[1]

II. Computational Method

A. Classical Interactions. In our calculations we employ Beeman's integration algorithm[20] as a good compromise between stability, accuracy, and the required computer time. This method gives the same positions as the Verlet algorithm and it is time reversal invariant. For the calculation of the forces in the neutral Xe clusters we use a 2-body potential derived by Barker, Klein, and Robetic.[3] This potential was obtained by fitting a variety of experimental data such as the dilute gas viscosity, the second virial coefficient, the vibrational level spacings of the dimers, and the differential collision cross sections, along with the zero temperature, zero pressure lattice spacing in the solid. We choose to perform our calculations using the Barker et al. potential because of its reported agreement with a wide range of experimental measurements. In the majority of the previous calculations, the Lennard-Jones 6-12 potential for xenon was used. The relative features of the two potentials are depicted in Figure 1.

The calculation of the electrostatic part of the energy is based on the assumption that the induced dipole moment $\vec{d}_i(\vec{r}_i)$ of the Xe atom at the point $\vec{r}_i$ is a linear function of the total electric field at that point $\vec{E}^t(\vec{r}_i)$. Furthermore, since the Xe atoms have their valence shell filled they do not have any preferable polarization direction. Thus, the induced dipoles are oriented

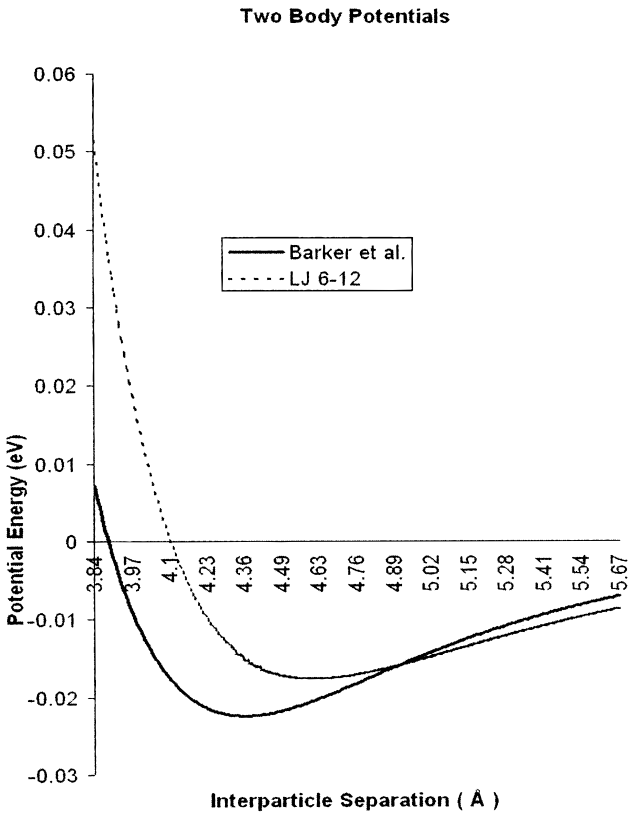

Figure 1. Xe−Xe potentials.

along the direction of the field.[21] Denoting by α the atomic mean polarizability, we write

$$\vec{d}_i(\vec{r}_i) = \alpha \vec{E}^t(\vec{r}_i) \tag{1}$$

The actual electric field at each point is the sum of the Coulombic field due to the charges $\vec{E}^c(\vec{r}_i)$ and the field generated by the dipoles $\vec{E}^d(\vec{r}_i)$:

$$\vec{E}^t(\vec{r}_i) = \vec{E}^c(\vec{r}_i) + \vec{E}^d(\vec{r}_i) \tag{2}$$

Denoting by q_j the total charge on the jth atom and with $\vec{r}_{ij} = \vec{r}_i - \vec{r}_j$ we have

$$\vec{E}^c(\vec{r}_i) = -\sum_{j\neq 1} \frac{q_j \vec{r}_{ij}}{|r_{ij}|^3} \tag{3}$$

$$\vec{E}^c(\vec{r}_i) = -\sum_{j\neq 1} \left[\frac{\vec{d}_j(\vec{r}_j)}{|r_{ij}|^3} - \frac{3[\vec{d}_j(\vec{r}_j)\cdot\vec{r}_{ij}]\vec{r}_{ij}}{|r_{ij}|^5} \right] \tag{4}$$

Substituting eqs 1, 2, and 3 into eq 4 and rearranging results in

$$\vec{d}_i(\vec{r}_i) + \alpha \sum_{j\neq 1} \left[\frac{\vec{d}_j(\vec{r}_j)}{|r_{ij}|^3} - \frac{3[\vec{d}_j(\vec{r}_j)\cdot\vec{r}_{ij}]\vec{r}_{ij}}{|r_{ij}|^5} \right] = \alpha \sum_{j\neq 1} \frac{q_j \vec{r}_{ij}}{|r_{ij}|^3} \tag{5}$$

The above equations form a set of $3N$ equations for the x,y,z components of the N dipoles. Representing all $\vec{d}_i$'s as a $3N$-dimensional vector D, this set can be written in matrix form:

$$A \cdot D = Q \tag{6}$$

The elements A_{ij} and Q_j can be obtained directly from eq 5.

The electrostatic energy of the system with the above-described interactions consists of three parts:[22]

1. The interaction energy between the dipoles and the Coulombic field due to the charges:

$$V_1 = -\sum_{i=1}^{N} \vec{d}_i(\vec{r}_i)\cdot\vec{E}^{c}(\vec{r}_i) \tag{7}$$

2. The interaction energy of the dipoles themselves:

$$V_2 = -{}^1/_2 \sum_{i=1}^{N} \vec{d}_i(\vec{r}_i)\cdot\vec{E}^{d}(\vec{r}_i) \tag{8}$$

where the factor $^1/_2$ prevents the double counting of each pair of dipoles.

3. The work of polarization. To calculate the work done by the field to separate the charges inside the induced dipole, we first assume that the gradient of the field does not vary significantly on the scale of the atomic dimensions and therefore can be considered uniform inside each atom. Next we consider that the polarizable atom acquires its final dipole moment under the influence of an external field, smoothly switched on and slowly increased from zero to its actual value. At each time during this process the dipole moment will be proportional to the applied field and the work done is

$$V_3 = \int_0^{\vec{E}^{t}(\vec{r}_i)} \alpha\vec{E}'(\vec{r}_i)\, \mathrm{d}\vec{E}'(\vec{r}_i)$$

$$= {}^1/_2 \sum_{i=1}^{N} \vec{d}_i(\vec{r}_i)\cdot\vec{E}^{t}(\vec{r}_i) \tag{9}$$

Therefore the total electrostatic energy is

$$V^{el} = V_1 + V_2 + V_3 = -{}^1/_2 \sum_{i=1}^{N} \vec{d}_i(\vec{r}_i)\cdot\vec{E}^{c}(\vec{r}_i) \tag{10}$$

We calculate the N dipoles at each time step by inversion of the matrix A, and then we calculate the electrostatic potential and the corresponding force. The inverse matrix A^{-1} is calculated explicitly because we need it for the calculation of the electrostatic forces, otherwise we could employ more efficient iterative techniques for the calculation of the dipoles. The charge is entirely localized at one Xe atom. In order to simplify our calculations, we assume, for computational convenience, that the polarizability of the ion is the same as for the neutral atoms, that is, equal to 4.1 Å^3.[23] The actual polarizability of the ion is different than the polarizability of the neutral atoms but since the field of the charge is much stronger than the field of the induced dipoles, this approximation does not affect the calculated electrostatic energy. We test this by varying the value of the polarizability of the ion and we find that the electrostatic energy remains practically the same. The Coulombic field at the ion is taken to be zero.

In the Appendix, in order to test the validity of the classical part of our model, we calculate the dielectric energy of a charged dielectric sphere as a function of the distance of the charge from the center. This energy is relative to the energy of the sphere with the charge placed at the origin. We compare this energy with the relative increase of the computed electrostatic energy of charged cluster Xe_{55}^+ with close-packing geometry as the location of the charge moves from the center to the surface of the cluster. The agreement of the two calculations is depicted in Figure 2. It is worth mentioning that the continuum case

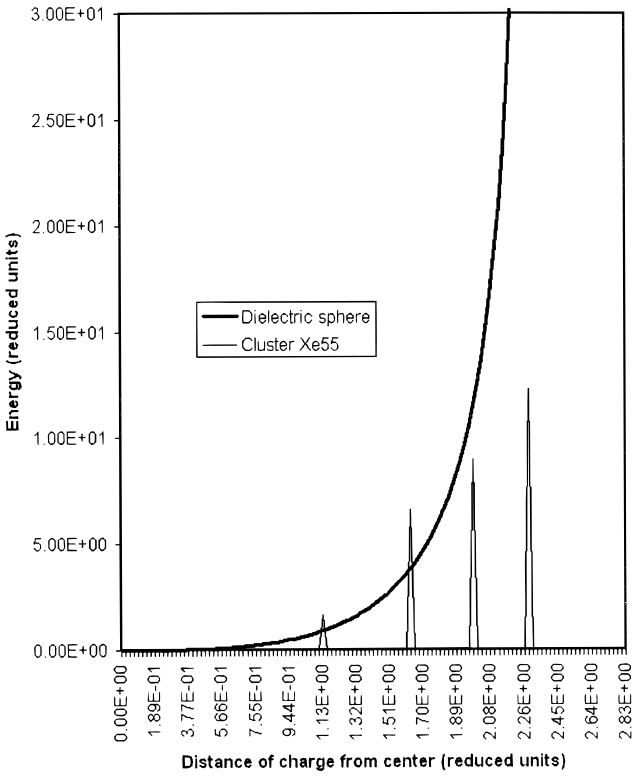

Figure 2. Dielectric sphere with a single charge: Electrostatic energy relative to the origin. (The reduced units are based on the Barker potential.)

energy possesses a singularity as the point charge reaches the surface of the sphere.

B. Quantum Hamiltonian. The systems we discuss are clusters with $N - 1$ neutral Xe atoms and one ion Xe^+. The migration of the charge inside the clusters occurs through electron exchange between the neutral atoms and the ion. In our approximation we consider that the mobile electrons of each atom occupy an averaged, rotationally invariant electronic state of the valence shell, which can take two possible spin values, either $s = +^1/_2$ or $s = -^1/_2$. Since the electronic transitions between these states inside the same atom do not result in physically distinguishable states for the clusters, we consider that at each atom there are only two mobile valence shell electrons having opposite spin values. We call these states *mobile electron valence shell states*. Therefore, we study the rearrangements of $2N - 1$ electrons in the $2N$, totally available states. It is convenient to describe our quantum mechanical calculations using second quantization notation. The vacuum state $|0\rangle$ is first defined as the state with no mobile valence electrons in any of the Xe atoms in a cluster. The electron creation, $a_{is}^{\dagger}$, and annihilation, $a_{i,s}$, operators are defined by the equations:

$$a_{is}^{\dagger}|0\rangle = |i_0^{el}\rangle s \tag{11}$$

$$a_{i,s}|i_0^{el}\rangle s = |0\rangle \tag{12}$$

The state $|i_0^{el}\rangle$ describes an electron in a mobile valence state of the ith Xe atom and in the s spin state. The physical meaning of $a_{i,s}^{\dagger}$ is that it creates an electron in the previously empty s spin state of the ith atom and $a_{i,s}$ is that it destroys an existing electron in the s spin state at the ith Xe atom. We further define the state $|0'\rangle$ as

$$|0'\rangle = a^{\dagger}_{1,-1/2}a^{\dagger}_{1,+1/2} \ldots a^{\dagger}_{N,-1/2}a^{\dagger}_{N,+1/2}|0\rangle$$
$$= \prod_i \prod_s a^{\dagger}_{i,s}|0\rangle \quad (13)$$

This state represents a neutral xenon cluster. It is important to define the normal order of the product. We follow the convention that i increases from 1 to N, the cluster number, and for each i the spin states are taken in an ascending order. We introduce the quantum hole which simplifies our calculations. For any possible arrangement of the $2N - 1$ mobile valence shell electrons the hole is located at the vacant atom, i.e., the Xe ion, it has a positive charge $+e$ and a mass equal to that of an electron. The hole creation, $c^{\dagger}_{i,s}$, and annihilation, $c_{i,s}$, operators are defined by the equations

$$c^{\dagger}_{i,s} = (-1)^{(1/2)+s}a_{i,s} \quad (14)$$

$$c_{i,s} = (-1)^{(1/2)+s}a^{\dagger}_{i,s} \quad (15)$$

Applying $c^{\dagger}_{i,s}$ on the neutral cluster state $|0'\rangle$, we destroy the s spin electron which is located at the ith Xe atom and this is denoted by a state $|i_0\rangle$s:

$$c^{\dagger}_{i,s}|0'\rangle = |i_0\rangle_s \quad (16)$$

Similarly

$$c_{i,s}|i_0\rangle_s = |0'\rangle \quad (17)$$

The Hamiltonian we work with is referred to as the Hubbard Hamiltonian. This is a model of isotropic electron hopping between different sites in a crystal lattice. The electrons are assumed to be in a single band, and they interact only when they occupy opposite spin states of the same atom. It has been used in the study of electric and magnetic properties of solids and clusters[9,24,25] as well as of one- and two-dimensional model lattices.[26] We arrive at this model for the description of the charge migration inside the xenon clusters by making a series of approximations.

The mass of the Xe atoms is 5 orders of magnitude greater than the mass of the electron. The ground state of the clusters, which we calculate later, has an energy difference from the first excited state of the order of 1 eV. The spacing of the corresponding vibrational states of the nuclei, calculated from the neutral interaction potential in the harmonic approximation, is of the order of 0.05 eV. Therefore, the splitting of the states of the hole is strong enough that the motion of the nuclei will not affect their separation in a significant manner. We also find that the ground state of the hole is not degenerate, even when the atoms are occupying the exact sites of the two configurations that we use. Consequently, the clusters do not exhibit the Jahn−Teller effect. These observations validate the Born−Oppenheimer approximation, according to which we consider the electronic states parametrically dependent on the motion of the nuclei. Furthermore, we assume that the motion of the nuclei obeys the laws of classical mechanics.

The frozen core approximation implies that the core electrons have much higher excitation energies than the valence electrons and their states are not affected by the interatomic distance. They can be treated as a charge distribution with Pauli exclusion forces that causes a repulsive potential for the motion of the valence electrons. The valence electrons experience a pseudopotential given by the average of this repulsive potential of the core electrons and their interaction with the nucleus.

Next we employ the tight binding approximation. If the Xe atoms are very far apart, the hole will be located at a certain site and this situation will be represented with the state $|i_0\rangle_s$, with i labeling the ion Xe^+ and s the spin state of the vacant orbital. As we lower the spacing of the sites these states will eventually start overlapping and will no longer be orthogonal. This overlapping is the result of the electron exchange integral between the ion and the neighboring atoms. If this overlap is small, tight binding limit, we can ignore the excited states of the Xe atoms and we can construct an orthogonal basis set $\{|i\rangle_s\}$ as follows:

$$|i\rangle_s = |i_0\rangle_s - {}^1/_2 \sum_{j\neq 1} N_{ij}|j_0\rangle_s \quad (18)$$

with $N_{ij} = \langle i_0|j_0\rangle$. The orthogonality of these states to the first order of N_{ij} is

$$\langle j|i\rangle = \langle j_0|i_0\rangle - {}^1/_2 \sum_{k\neq j} N_{jk}\langle j_0|k_0\rangle - {}^1/_2 \sum_{l\neq j} N_{li}\langle l_0|i_0\rangle + {}^1/_4 \sum_{k\neq j}\sum_{l\neq j} N_{jk}N_{li}\langle j_0|k_0\rangle\langle l_0|i_0\rangle = 0 + O(N_{ij}{}^2) \quad (19)$$

$$\langle i|i\rangle = 1 + O(N_{ij}{}^2) \quad (20)$$

Our model Hamiltonian will be constructed as being diagonal in the $\{|i\rangle\}$ representation.

The Hamiltonian, in which we incorporate all the above assumptions, in the second quantization notation is

$$H = \sum_s \sum_i c^{\dagger}_{i,s}c_{i,s}V^{\mathrm{el}}_i(R) + {}^1/_2 \sum_{s,s'} \sum_{i<j} [c^{\dagger}_{i,s}c_{j,s'} + c^{\dagger}_{j,s'}c_{i,s}]h(r_{ij}) \quad (21)$$

The first term of this Hamiltonian corresponds to the diagonal matrix elements in the $\{|i_0\rangle_s\}$, *the nonoverlapping states* representation. The V^{el}_i is the electrostatic energy of the cluster for the charge located at the ith Xe atom, and R is a $3N$-dimensional vector denoting the positions of the N atoms.

The second term corresponds to the nondiagonal elements in the $\{|i_0\rangle_s\}$ representation. The $h(r_{ij})$ is the hopping energy between the ith and jth atoms. This is half of the energy difference between the $\mathbf{I}(^1/_2)_g$ and $\mathbf{I}(^1/_2)_u$ states of $Xe_2{}^+$. The data are taken from the $Xe_2{}^+$ potential curves derived by Wadt.[27] There are three dipole-allowed transitions for $Xe_2{}^+$: $\mathbf{I}(^1/_2)_u \rightarrow \mathbf{I}(^3/_2)_g$, $\mathbf{I}(^1/_2)_u \rightarrow \mathbf{I}(^1/_2)_g$, and $\mathbf{I}(^1/_2)_u \rightarrow \mathbf{II}(^1/_2)_g$. The first two dissociate in the same asymptote Xe + $Xe^+(^2P_{3/2})$, but the $\mathbf{I}(^1/_2)_u \rightarrow \mathbf{I}(^3/_2)_g$ is very weak and we have neglected its contribution. Of course, this, as well as the other approximations we have used, need to be verified eventually with more detailed calculations. The third, $\mathbf{I}(^1/_2)_u \rightarrow \mathbf{II}(^1/_2)_g$, dissociates in the Xe + $Xe^+(^2P_{1/2})$ asymptote, which is ~1.5 eV above,[27] 10 times higher than the total binding energy per atom in the studied clusters. The hopping energy of the $\mathbf{I}(^1/_2)_u \rightarrow \mathbf{I}(^1/_2)_g$ transition is also used in a previous calculation[7] and it allows a direct comparison of our results with theirs.

It is worth mentioning that our Hamiltonian for the singly-charged clusters can be reduced to the Hückel Hamiltonian[28] under the assumption that the hopping of the hole occurs only between the nearest-neighbor xenon atoms and that all the sites are equivalent. The first assumption is physically reasonable for our clusters, since the hopping potential becomes almost zero for interparticle separations greater than the nearest-neighbor distance, but the second one neglects the role of the

polarization field which drives the charge toward the center of the cluster. The Pariser−Parr−Pople[29] model, which allows the sites to differ from one another, and, in addition to the Hückel model features, includes the interactions between the hopping charges, is equivalent to our Hamiltonian. The similarity of these models for spin-free systems has already been shown.[30,31]

We assume that the induced dipoles are instantaneously oriented toward the charged atom. This assumption is warranted by the relative magnitudes of the hopping frequency $\omega_h = h(r_{ij})/2\hbar$ and the characteristic frequencies of the electronic spectrum of Xe. In particular, the time-dependent atomic polarizability is

$$\alpha(\omega) = \frac{e^2}{m_e} \sum_n \frac{f_{n0}}{{\omega_{n0}}^2 - \omega^2} \tag{22}$$

where e and m_e are the electron charge and mass, respectively, and ω_{n0} is the Bohr frequency between the nth excited state and the ground state of Xe, f_{n0} the oscillator strength, and ω the frequency of the electric field. The Xe atom's first persistent spectral line is at 2.65 eV, thus all ${\omega_{n0}}^2$ are greater than 10^{31} s^{-2}. We consider the frequency of the electric field equal to the hopping frequency of the hole. The maximum value that it can take is at the minimum of the ground state $\mathbf{I}(^1/_2)_u$, and its square is ${\omega_h}^2 \simeq 10^{29}$ s^{-2}, 2 orders of magnitude smaller than ${\omega_{n0}}^2$. Therefore, we can neglect the dependence of the polarizability on the frequency of the charge motion.

In our calculations we did not take into account any coupling between spin and position states. It is also important to emphasize that our Hamiltonian describes the charge hopping in an isotropic manner. The hopping probability of the hole between any two atoms depends exclusively on their distance, and it is not affected by their relative orientation. Of course this is not true in the real clusters, since p states are involved and the hopping energy must depend on the orientation of the atoms.

At each time step we derive the matrix elements of our Hamiltonian in the $\{|i_0\rangle_s\}$ representation. We solve for the ground state eigenvector $\Psi(R)$ and the two lower eigenvalues, $E^0(R)$ and $E^1(R)$, using the Lanczos method.[32] According to the Born−Oppenheimer approximation the xenon atoms experience a potential equal to the ground state energy of the hole. The force which is exerted on the ith atom with coordinates (x_i,y_i,z_i) is

$$\vec{F}_i(R) = -\nabla_i E^0(R) \tag{23}$$

We calculate each component of the force vector, applying the extended Hellman−Feynman theorem.[28] This theorem states that if $\Psi(x)$ is an eigenvector of the Hamiltonian $H(x)$, then

$$\frac{\partial}{\partial x}\langle\Psi(x)|H(x)|\Psi(x)\rangle = \left\langle\Psi(x)\left|\frac{\partial}{\partial x}H(x)\right|\Psi(x)\right\rangle \tag{24}$$

Our code evaluates the matrix for the three components of the N force operators, in the $\{|i_0\}\rangle_s$ representation. The expectation values of these matrices are obtained by right and left multiplication with the ground state eigenvector.

III. Results

A. Molecular Dynamics Calculations. In our molecular-dynamics calculations, we use two different methods of generating the initial configurations. First, we equilibrate the neutral clusters at a certain temperature, by proper scaling of the velocities of the atoms at each step, and we use these positions and velocities of the Xe atoms as initial conditions for the charged cluster molecular dynamics. These calculations simulate the experimental situation for short times after the ionization process. As a measure of the stability of the clusters we consider the distance of the most distant atom from the center of mass of the cluster. We monitor this distance at each time step, and if it increases linearly, we know that fragmentation or sublimation has occurred. Clusters made with this method are unstable. After a few picoseconds, they evaporate by releasing one surface atom. The lifetimes of these clusters do not possess any accordance with the magic numbers pattern.

These results are in line with previously reported experimental[33] and computational[34] studies. In general, just above the ionization threshold the binding energy of the neutral clusters should prevent fragmentation. However, the binding energy of small rare gas neutral clusters is smaller than the average photon energy and "none of the experimental spectra can be considered free of fragmentation effects".[33] In a recent computational study,[34] it is reported that clusters Xe_n^+, $n < 55$, are subject to rapid evaporation within few picoseconds after their ionization, and their size reduction continues until they thermalize. Only very large clusters, such as Xe_{55}^+, maintain their original size and simply heat up after ionization.

In the second approach we equilibrate the charged clusters at the desired temperatures, and we use these positions and velocities of the atoms as the initial conditions for our molecular dynamics calculations. This technique simulates the experimental situation for times long enough for the precursor cluster to accommodate the excess of energy, which is released after the ionization, by successive evaporations and/or fragmentations. These clusters are very stable and for temperatures lower than a third of ϵ/k ($\sim$70 K) they do not show any tendency to evaporate after times that can be as long as several hundreds of picoseconds, regardless of the cluster number.

In both approaches, we notice that the ground state vector does not possess a firm fixed structure for temperatures greater than 10 *K*. This is true for both the icosahedral geometry and the close-packing one. We calculate the charge probability distribution over the xenon atoms at each time step. In all the cases we studied we did not find any evidence of a permanent dimer. Instead we observed dimers, trimers, tetramers, etc. that appeared as peaks in the probability distribution for certain times and disappeared later on without following any particular pattern.

The results of our calculations, of course, cannot prove whether or not a dimer forms inside a real cluster. Nevertheless, our model contains explicit physical assumptions that previous authors have used to support the dimer formation;[5,7,35] namely, we calculate the electrostatic interactions using a point polarizability model, and we assume that the hopping occurs by the transition between the ground state and the first nonbonding state of the Xe_2^+.

B. Simulated Annealing Calculations. We use our molecular dynamics code to perform simulated annealing calculations. This is a minimization method which simulates the thermodynamic process of the slow cooling of a system: The slow rate of lowering the temperature diminishes the probability of ending up in local minima and metastable states when searching for the global minimum of the energy. We start with initial velocities sampled from a Maxwell distribution corresponding to a temperature which allows large displacement of the Xe atoms from their equilibrium positions. We use as initial

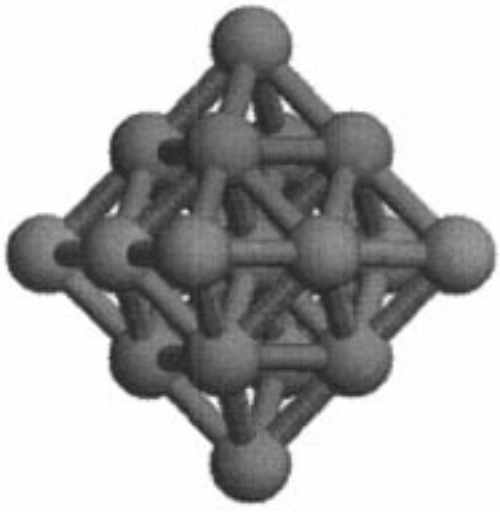

Figure 3. Initial configuration of cluster with 19 atoms and close-packing (CP) geometry.

TABLE 1: Calculated Minimum Energies for Neutral and Charged Clusters

	IC geometry		CP geometry	
cluster size	charged	neutral	charged	neutral
10	−1.977	−0.579	−2.034	−0.591
11	−2.170	−0.658	−2.183	−0.672
12	−2.272	−0.759	−2.371	−0.777
13	−2.510	−0.900	−2.597	−0.905
14	−2.580	−0.953	−2.748	−1.006
15	−2.675	−1.029	−2.896	−1.108
16	−2.774	−1.107	−3.04	−1.212
17	−2.928	−1.186	−3.183	−1.312
18	−3.009	−1.289	−3.323	−1.414
19	−3.190	−1.430	−3.463	−1.517
20	−3.252	−1.478	−3.561	−1.597
21	−3.330	−1.546	−3.69	−1.700

positions for the atoms inside the clusters both the icosahedral (Figures 5 and 6) and the close-packing geometries (Figure 3). The minimum value we find for each cluster number from 10 to 21 is listed in Table 1 for clusters with both geometries. We cool the clusters by removing kinetic energy through scaling of the velocities at each time step. We use various scaling rates and initial sampling temperatures. For each cluster number and each geometry, we keep the lowest potential we find as its ground state. These measurements are used for the calculation of the sublimation energy and of the binding energy of the charged clusters. The sublimation energy for the cluster number N is calculated by

$$E_{sub}(N) = |E_{min}(N) - E_{min}(N-1)| \qquad (25)$$

When the close-packing geometry is used, we cannot find a stable 19 particle cluster. There is a sharp maximum at the cluster number 13 and then the sublimation energy falls monotonically. The results are similar for the Lennard-Jones 6-12 potential. When we use the icosahedral geometry, we derive two distinct maximum values of the sublimation energy for the 13 and 19 cluster numbers. The relative values of the sublimation energy that we calculate are in absolute agreement with previously reported values which were derived using a Lennard-Jones 6-12 potential and the same geometrical structures.[1] The complete investigation of the dependence of the stability of the magic numbers clusters on their geometry is beyond the scope of this work. We restrict ourselves to the study of the effect of the charge and its hopping on the stability of the Xe clusters. We test how these factors modify the pattern of the sublimation energy.

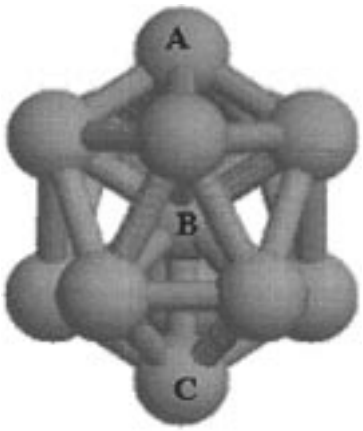

Figure 4. Initial configuration of cluster with 13 atoms and icosahedral (IC) geometry.

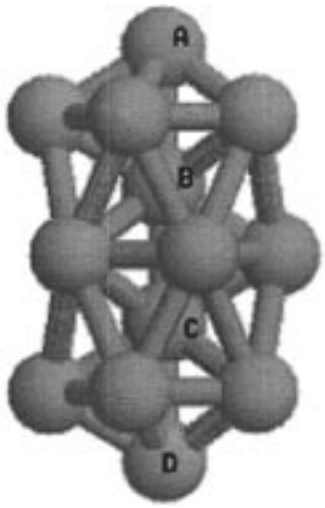

Figure 5. Initial configuration of cluster with 19 atoms and icosahedral (IC) geometry.

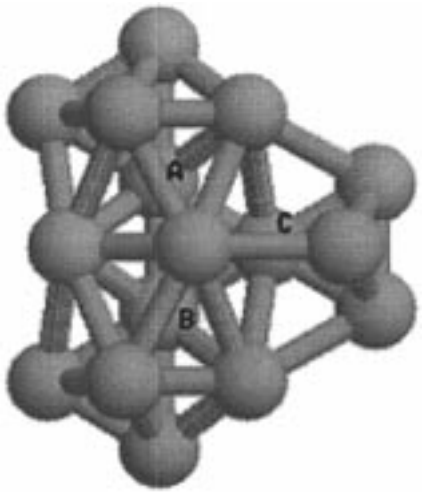

Figure 6. Initial configuration of cluster with 23 atoms and icosahedral (IC) geometry.

As Figure 7 shows, the sublimation energy possesses two distinct maxima for the cluster numbers 13 and 19 when the icosahedral geometry is used. This can be directly associated with the experimentally observed stability of charged clusters with cluster numbers 13 and 19. The pattern of the sublimation

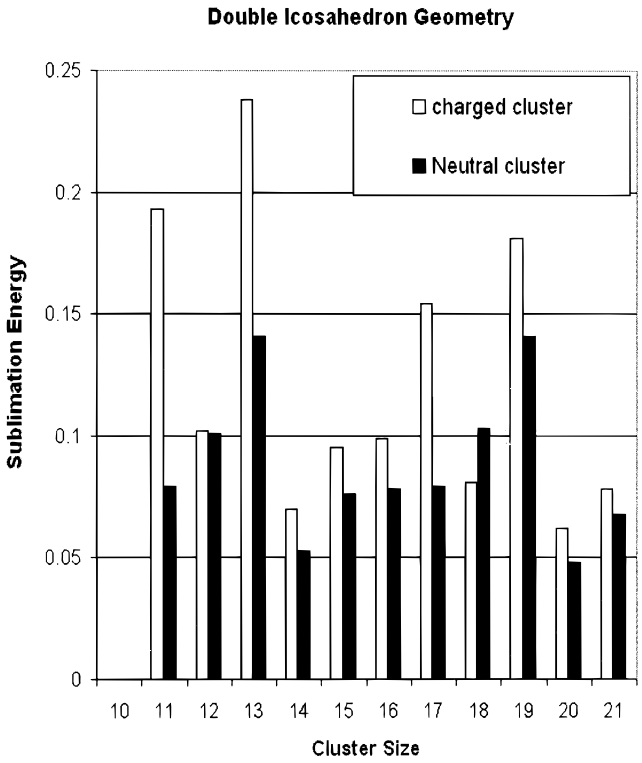

Figure 7. Sublimation energies for neutral and charged icosahedral (IC) clusters.

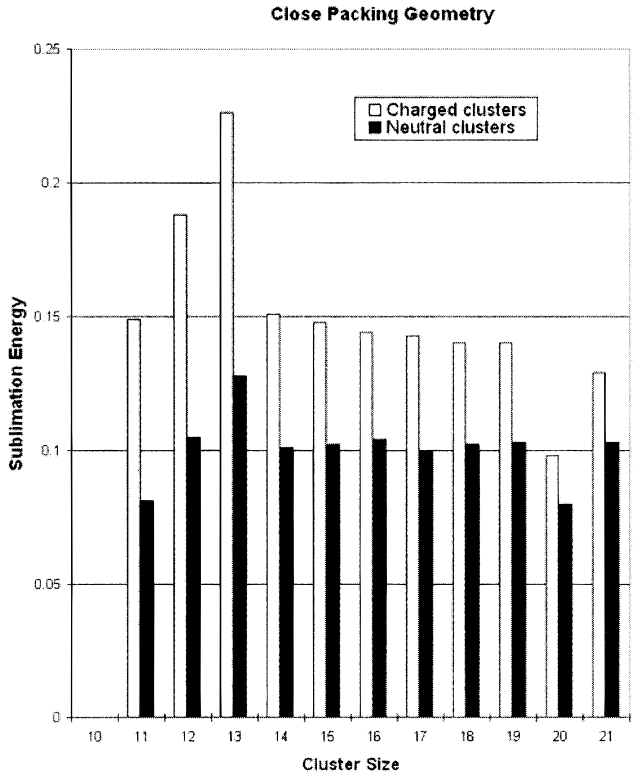

Figure 8. Sublimation energies for neutral and charged close-packing (CP) clusters.

energy versus cluster numbers is changed from that of the neutral clusters which is also depicted in the same figure, but it still has the two maxima corresponding to the first two magic numbers.

When the close-packing geometry is employed, Figure 8, the inclusion of the electrostatic interaction and the Quantum effects does not change the pattern of the sublimation energy. The

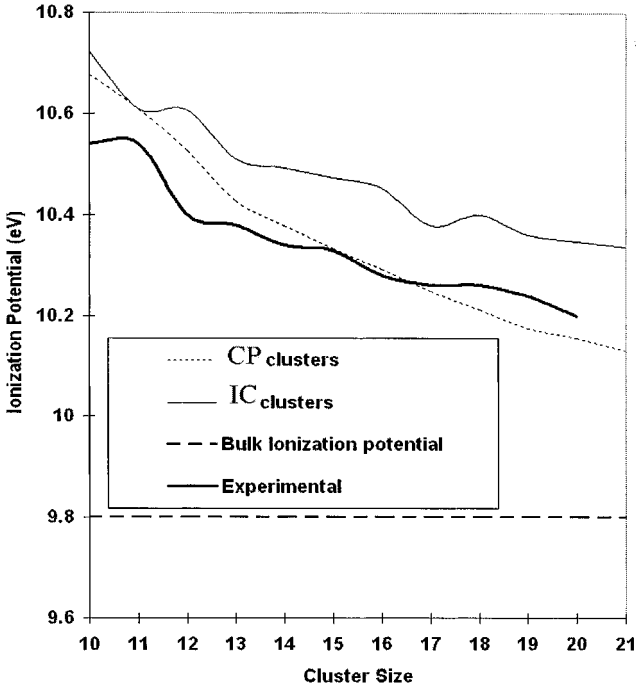

Figure 9. Adiabatic ionization potential.

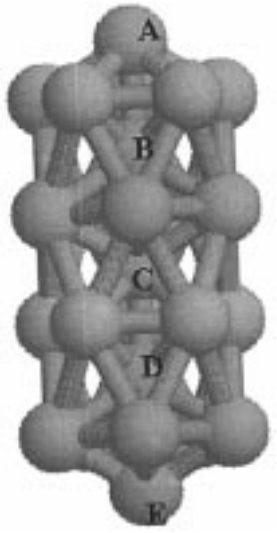

Figure 10. Cluster of 25 Xe atoms with icosahedral geometry and two attached pentagonal caps.

sublimation energy is simply moved to higher values, as we include these factors, without changing its dependence on the cluster number. As in the case of the neutral clusters, only the stability of the magic number 13 is predicted.

From the same calculations, we derive asymptotically the adiabatic ionization potential in the bulk as the difference between the atomic ionization potential and the binding energy. The binding energy is equal to the difference between the minimum energy of the charged and neutral cluster, for which the experimental value is 9.8 eV.[18] For clusters with 21 atoms our model gives 10.1 eV for the Close-Packing geometry and 10.3 eV for the icosahedral geometry (Figure 9). The values of the ionization potentials for clusters from 10 to 20 are also in good agreement with experimental results.[19] These values have an average difference of 0.14 eV from the calculated values with icosahedral geometry and 0.05 eV for the close-packing one. Nevertheless, the pattern of the experimental values seems closer to that of the icosahedral geometry.[9] These experimental

results have an uncertainty equal to 0.1 eV. An electronic structure calculation has been published that considers the delocalization of the hole along one direction due to the p nature of the empty orbital.[36] According to this work, the charged clusters of up to 19 atoms consist of either a Xe_3^+ or Xe_4^+ surrounded by polarized neutral atoms. The calculated adiabatic ionization potential for the Xe_{19}^+ by this model is 10.1 eV, the corresponding value we calculate is 10.3 eV (for the icosahedral geometry). The agreement of these values gives us confidence that our isotropic hopping approximation describes the essential physics of the charged clusters.

The ground state eigenvector $|\Psi_0(R,s)\rangle$ expanded in terms of our basis set is

$$|\Psi_0(R,s)\rangle = \sum_{i=1}^{N} b_i |i_0\rangle_s \tag{26}$$

Consequently, the probability of finding the hole located at the ith atom is equal to $|b_i|^2$. Our code calculates the distribution of this probability over all the Xe atoms of the clusters at each time step. A dimer would be manifested by two large peaks in this distribution at the atoms which would constitute the dimer. In addition, we would expect that the distance between these two particular atoms to be smaller than the average nearest-neighbor distance and closer to the interparticle separation in the Xe_2^+ molecular ion. In our simulated-annealing calculations on clusters with close-packing geometry we did not find any evidence of dimer formation. In the case of clusters with icosahedral geometry we did not find dimer formation for clusters having up to 17 Xe atoms. For cluster numbers 18, 19, and 20, the probability distribution possesses relatively higher values at the two Xe atoms, which are in the interior of the clusters, denoted by B and C in Figure 5. However, the distance between these two atoms did not become smaller, and the clusters retained their icosahedral geometry. In all our simulated annealing calculations, the atoms are free to move in any direction that lowers the energy of the clusters, and there is not any constraint to maintain the geometrical structure. As the cluster number increases to 23, a cluster configuration that corresponds to a closed shell of the icosahedral geometry (Figure 6), the two peaks at the labeled atoms A and B become even smaller, and a third weak peak appears at the atom C.

In order to search for the possibility that the formation of a dimer corresponds to a local minimum of the potential energy, we performed calculations with initial conditions propitious to dimer formation. In particular, we started our calculations with the two atoms (B and C in Figure 5) close to each other at the separation distance of the minimum of energy of Xe_2^+. We also adjusted the positions of the other atoms in order to keep their interaction with the dimer in the bound regime of the Barker et al. potential. The result of the simulated-annealing with this initial configuration was that the two atoms, which were in close proximity in the beginning, moved apart, approaching the separation that the icosahedral geometry provides for them.

C. Hole Hopping Directionality. In the real clusters, the hopping of the charge between the xenon atoms must depend on the relative orientation of their p orbitals. The isotropic hopping of our model cannot describe this effect. The explicit account of the p orbitals would increase considerably the dimensionality of the problem and the computing time of our calculations. As an alternative we performed a series of calculations restricting the hopping only in one direction as a limiting case of the effect of the p character of the empty orbital.

TABLE 2: Charge Probability Distribution: Directional Hopping, IC Geometry

cluster size	hopping sites	% probability per site				
13 (Figure 4)	3	A	B	C		
		11.7	76.54	11.7		
19 (Figure 5)	4	A	B	C	D	
		4.35	45.64	45.64	4.35	
25 (Figure 10)	5	A	B	C	D	E
		1.92	25.03	44.83	25.03	1.92

We used the icosahedral geometry for clusters of up to 19 atoms. We further continued building artificial clusters of up to 25 atoms by adding a pentagonal cap along the hopping axis. The hopping axis was chosen to be the line which joins the interior atoms in the Xe_{19}^+ (B and C in Figure 5) and is taken to be the z axis. We call the atoms that lay on this axis *axial*, and the rest *peripheral*. We arrived at this approximation by considering the following:

i. The overlap of the p_z orbitals of the peripheral atoms is zero. The overlap of their p_x and p_y orbitals with the p_z of the axial atoms is 10 times smaller than the p_z overlap of the axial atoms,[36] and in a first approximation it can be neglected.

ii. The charge exchange lowers the energy of the clusters. Therefore, we assume that the charge must be delocalized preferably along the direction on which lies the maximum number of atoms, the z axis that we defined above.

We calculate the probability distribution of the charge distribution over the atoms which lay on the hopping axis, and the results are in Table 2. In these measurements it is clear that the delocalization is counterbalanced by the forces that the induced dipoles exert on the charge. The electrostatic energy takes its minimum value when the charge is located at the center of mass of the clusters. Therefore, the induced dipoles tend to localize the charge at this point, opposing an equipartition of the charge probability over the axial atoms. These results also show that a dimer forms as a special case only when the number of the axial atoms is even.

IV. Conclusions

The validity of our model is ascertained by the agreement of the adiabatic ionization potentials, which we calculate, with the experimental values.[18,19] The binding energies that our model results in are very close to the corresponding values which were derived by other authors in purely quantum mechanical calculations, explicitly accounting for the p character of the empty orbital.[36] This means that the isotropic hopping of the charge is an adequate approximation for this level of calculations.

Our model does not result in any dimer formation. Conversely, the ground state of our Hamiltonian, at temperatures close to zero, reflected a spherically symmetric delocalization of the charge around the central atom, for clusters with the close-packing geometry. The radial distribution of the charge probability showed that the most probable location for the charge was the central atom of the cluster. For the rest of the atoms, as their distance from the center increased, the probability to carry the charge decreased rapidly. These results were consistent with our calculation of the electrostatic energy of a singly-charged dielectric sphere as a function of the distance of the charge from the center, a continuous matter limit of the clusters. For clusters with the icosahedral geometry structure the charge probability distribution differs with the size of the cluster and it possesses one maximum for clusters up to 17 atoms, two for 18, 19, and 20 atoms and three for 21, 22, and 23 atoms. Again no dimer was found for these clusters.

The formation of the dimer in the work of previous authors provided a straightforward method to include in the energy of the clusters the charge exchange energy. Without this term the calculated binding energies of the clusters, and consequently the ionization potential, are in noticeable disagreement with the experimental values. But the assumed dimer required drastic modifications of the parameters of the classical potential. The new parameters for the interaction of the dimer with the surrounding neutral atoms have not been studied at the same level as the parameters for the interaction between the neutral atoms, and therefore they must include additional approximations. Our model does not require any further assumptions for the classical part of the Hamiltonian and the exchange energy of the charge is calculated quantum mechanically in an independent manner.

As for the understanding of the magic number pattern, our model provides a plausible way to associate the magic numbers with the maxima of the sublimation energy that the icoshedral geometry provides. This is so because the hopping of the charge, and consequently the probability distribution of the charge over the atoms inside clusters, do not cause any dislocations in the geometrical structure. Our results show that the sublimation energies of the neutral clusters and those of the charged clusters follow the same pattern, the latter being just shifted above the former. Therefore, the detected magic numbers for the charged clusters can be related to the stability of neutral clusters of the same size, though they do not reflect the stability of the precursor clusters which fragment after ionization. The dimer assumption of the previous authors requires a revised geometry for the charged clusters, since the two Xe atoms of the dimer are 40−50% closer than the average nearest-neighbors separation.[27] The dimer must be the central core around which the other atoms are attached. In this case the observed magic numbers cannot any longer be associated with the closed shells of the icosahedral geometry.

We plan to expand our model toward the description of doubly charged clusters. This will allow us to study the coulombic explosion that occurs in these clusters. Furthermore, we plan to test the applicability of this model for other rare gas clusters, such as Ar and Kr.

Acknowledgment. This work was supported in part by consecutive Dyson College Summer Research Grants and by National Science Foundation Grant No. CHE-9407309. D.C.A. gratefully acknowledges John C. Powers Jr. and Charles Masiello for their support.

Appendix: The Dielectric Sphere

Here we solve a continuous matter problem, in order to examine the analogies of its solution with the results of our model. We consider a sphere with a dielectric constant ϵ, a radius $R = 1$, and one point charge $+e$ located at a distance s from the center of the sphere. The choice of the coordinate system is such that the center of the sphere coincides with the origin, and the charge is on the positive z-axis. The dielectric constant was calculated from the atomic polarizability of Xe through the Clausius−Mossotti equation.

The potential of a point charge inside a dielectric sphere satisfies Poisson's equation inside the sphere

$$\nabla^2\Phi(\vec{r}) = -(4\pi e\delta^3(\vec{r} - \vec{s})/\epsilon) \tag{27}$$

and Laplace's equation outside

$$\nabla^2\Phi(\vec{r}) = 0 \tag{28}$$

The usual Coulomb point charge potential satisfies Poisson's equation, so the general solution inside is a sum of the Coulomb term and a solution of Laplace's equation. Expanding in Legendre polynomials, we get

$$\Phi_{\text{in}} = e\sum_l b_l r^l P_l(\cos\theta) + \frac{e}{\epsilon|\vec{r} - \vec{s}|}$$

$$\Phi_{\text{out}} = e\sum_l c_l r^{-l-1} P_l(\cos\theta) \tag{29}$$

Using the usual expansion of the Coulomb potential and matching normal $\vec{D}$ and tangential $\vec{E}$ at $r = 1$ gives

$$b_l + \frac{s^l}{\epsilon} = c_l$$

$$\epsilon l b_l - (l+1)s^l = -(l+1)c_l \tag{30}$$

with the solution

$$c_l = \frac{(2l+1)s^l}{\epsilon l + l + 1}$$

$$b_l = \frac{(\epsilon - 1)(l+1)s^l}{\epsilon(\epsilon l + l + 1)} \tag{31}$$

The total energy for a charge distribution is

$$W = -\frac{(\epsilon - 1)e^2}{8\pi}\int \mathrm{d}^3 r\,\vec{\nabla}\Phi\cdot\vec{\nabla}\Phi_{\text{c}}$$

$$= -\frac{(\epsilon - 1)e^2}{8\pi}\left(\int \mathrm{d}^3 r\,\vec{\nabla}\Phi\cdot[\Phi\vec{\nabla}\Phi_{\text{c}}] - \int \mathrm{d}^3 r\,\Phi\nabla^2\Phi_{\text{c}}\right) \tag{32}$$

The first term can be converted into a surface integral using the divergence theorem, and evaluated as

$$\frac{(\epsilon - 1)e^2}{2}\sum_l \frac{l+1}{\epsilon l + l + 1}s^{2l}$$

The second term is infinite for a point charge. If the charge is smeared out using, for example, a Gaussian distribution, the solution can be taken through exactly as above. The solution of Poisson's equation in an infinite dielectric is $\mathrm{erf}(|\vec{r} - \vec{s}|/w)/|\vec{r} - \vec{s}|$, where w is proportional to the width of the Gaussian, and erf is the error function. We want to eventually take the limit that the width goes to zero. If the width is small compared to the distance to the surface of the sphere, then the difference between the potential from this Gaussian charge distribution and a point charge will be given by exponentially small terms. Therefore, in the limit of small width, the b_l and c_l terms are identical to those calculated with a point charge, and the first term calculated above is independent of the Gaussian width for small enough widths. The second term is the integral over the Gaussian and the potential. This contains two terms. The first is the integration of the Gaussian and the error function above. Since these are both terms that are centered at $\vec{s}$, and the Gaussian goes to zero rapidly with distance, this integration is independent of the position of the charge. As the width goes to zero it diverges. The other term is well behaved in the limit of the Gaussian going to zero and evaluates to

$$-\frac{(\epsilon-1)e^2}{2}\sum_l \frac{(\epsilon-1)(l+1)s^{2l}}{\epsilon(\epsilon l+l+1)} \tag{33}$$

Combining these two terms gives the result

$$W = C + \frac{(\epsilon-1)e^2}{2\epsilon}\sum_l \frac{(l+1)s^{2l}}{\epsilon l+l+1} \tag{34}$$

where C is the self-energy which goes to infinity as the Gaussian width goes to zero, but is independent of position. Taking the difference in energy (ΔW) between having the point charge at s and having it at the origin eliminates the first term.

The formula for ΔW, generalized for any sphere with radius R, becomes

$$\Delta W = \frac{(\epsilon-1)e^2}{2\epsilon}\sum_l \frac{(l+1)}{\epsilon l+l+1}\left(\frac{s}{R}\right)^{2l} - \frac{(\epsilon-1)e^2}{2\epsilon} \tag{35}$$

In order to compare this result with the electrostatic energy of the studied clusters, we calculate the radius as

$$R = \sigma(3N/4\pi)^{1/3} \tag{36}$$

where N is the number of atoms in the corresponding cluster and σ is the length unit.

The result for W for the charge inside the dielectric sphere is a hypergeometric function. The Bateman Manuscript Project Books define the ${}_1F_2(a,b;c;z)$ function to be

$${}_1F_2(a,b;c;z) = \sum_l \frac{\Gamma(a+l)\Gamma(b+l)\Gamma(c)}{\Gamma(a)\Gamma(b)\Gamma(c+l)l!}z^l \tag{37}$$

With $z = (s/R)^2$, we need the coefficients to agree to within a normalization of our coefficients

$$\frac{(\epsilon-1)(l+1)}{\epsilon(\epsilon\, l+l+1)} \tag{38}$$

Taking $a = 2$, we get

$$\frac{\Gamma(2+l)}{l!} = l+1 \tag{39}$$

This gives our $l+1$ term in the numerator. The term in the denominator must be constructed from the ratio of $\Gamma(b+l)$ and $\Gamma(c+l)$. For any value of d

$$\frac{d}{\epsilon l+l+1} = \frac{\Gamma\left(\frac{\epsilon l+l+1}{d}\right)}{\Gamma\left(\frac{\epsilon l+l+1}{d}+1\right)} \tag{40}$$

To get the hypergeometric formula, we need to choose $d = \epsilon + 1$. This means we must pick

$$b = \frac{1}{\epsilon+1}$$

$$c = \frac{\epsilon+2}{\epsilon+1} \tag{41}$$

We then get the result that

$${}_1F_2\left(2,\frac{1}{\epsilon+1};\frac{\epsilon+2}{\epsilon+1};s^2\right) = \frac{(\epsilon+1)\Gamma\left(\frac{\epsilon+2}{\epsilon+1}\right)}{\Gamma\left(\frac{1}{\epsilon+1}\right)}\sum_l \frac{l+1}{\epsilon l+l+1}s^{2l} = \sum_l \frac{l+1}{\epsilon l+l+1}s^{2l} \tag{42}$$

References and Notes

(1) Farges, J.; Feraudy, M. F.; Raoult, B.; Torchet, G. *Surf. Sci.* **1985**, *156*, 370.
(2) Barker, J. A. Interatomic potentials for inert gases from experimental data. In *Rare Gas Solids*; Klein, M. L., Venables, J. A., Eds.; Academic Press: New York, 1976; Vol. 1.
(3) Barker, J. A.; Klein, M. L.; Robetic, M. V. *IBM J. Res. Dev.* **1976**, *20*, 222.
(4) Soler, J. M.; Saenz, J. J.; Garcia, N.; Echt, O. *Chem. Phys. Lett.* **1984**, *109*, 71.
(5) Soler, J. M; Saenz, J. J.; Garcia, N. *Surf. Sci.* **1985**, *156*, 121.
(6) Soler, J. M; Saenz, J. J.; Garcia, N. *Chem. Phys. Lett.* **1985**, *114*, 15.
(7) Polymeropoulos, E. E.; Brickmann, J. *Surf. Sci.* **1985**, *156*, 563.
(8) Polymeropoulos, E. E.; Bopp, B.; Brickmann, J.; Jansen, L.; Block, R. *Phys. Rev. A* **1985**, *31*, 3565.
(9) Hubbard, J. *Proc. R. Soc. Ser. A* **1963**, *276*, 238.
(10) Echt, O.; Sattler, K.; Recknagel, E. *Phys. Rev. Lett.* **1981**, *47*, 1121.
(11) Harris, I. A.; Kidwell, R. S.; Nortby, J. A. *Phys. Rev. Lett.* **1984**, *53*, 2390.
(12) Rayane, D.; Melinon, P.; Cabeaud, B.; Hoareau, A.; Tribollet, B.; Broyer, M. *Phys. Rev. A* **1989**, *39*, 6065.
(13) Ding, A.; Hellich, J. *Phys. Rev. Lett.* **1983**, *94*, 54.
(14) Spear, W. E.; Le Comber, P. G. Electronic transport properties. In *Rare Gas Solids*; Klein, M. L., Venables, J. A., Eds.; Academic Press: New York, 1976; Vol. 2.
(15) Miller, L. S.; Howe, S.; Spear, W. E. *Phys. Rev.* **1987**, *166*, 871.
(16) Howe, S. H.; Le Comber, P. G.; Spear, W. E. *Solid State Commun.* **1971**, *9*, 65.
(17) Le Comber, P. G.; Loveland, R. J.; Spear, W. E. *Phys. Rev. B* **1975**, *11* (8), 3124.
(18) Schmenther, N.; Himpsel, E. J.; Soule, V.; Skibowski, M.; Steinman, N. *Phys. Rev. Lett.* **1975**, *34*, 528.
(19) Gantefor, G.; Broker, G.; Holub-Krappe, E.; Ding, A. *J. Chem. Phys.* **1989**, *91* (12), 7972−7977.
(20) Beeman, D. *J. Comput. Phys.* **1975**, *20*, 130.
(21) Gay, J. C.; Berne, B. J. *Phys. Rev. Lett.* **1982**, *49*, 194, 1982.
(22) Bottcher, J. C.; Bordewijk, P. *Theory of Electric Polarizability*. Elsevier: New York, 1952.
(23) Bell, R. J.; Zucker, I. J. Short and intermediate range forces. In *Rare Gas Solids*; Academic Press: New York, 1976, Vol. 1.
(24) Jones, W.; March, N. H. *Theoretical Solid State Physics*; Dover: New York, 1985.
(25) Callaway, J.; Chen, D. D.; Tang, R. *Phys. Rev. B* **1987**, *35*, 3705.
(26) Lee, M. A.; Motakabbir, K. A.; Schmidt, K. E. *Phys. Rev. Lett.* **1984**, *53*, 1191.
(27) Wadt, W. R. *J. Chem. Phys.* **1978**, *68* (2), 402.
(28) Levine, I. N. *Quantum Chemistry*; Allyn and Bacon: New York, 1983.
(29) Pariser, R.; Parr, R. G. *J. Chem. Phys.* **1953**, *21* (3), 466.
(30) Matsen, F. A.; Welsher, T. L.; Yurke, B. *Int. J. Quantum Chem.* **1977**, *12*, 985.
(31) Soos, Z. G.; Ramaseha, S. *Phys. Rev. B* **1984**, 29, 5410.
(32) Lanczos, C. *Applied Analysis*; Dover: New York, 1989.
(33) Kamke, W.; de Vries, J.; Krauss, J.; Kaiser, E.; Kamke, B.; Hertel; I. V. *Z. Phys. D* **1989**, *14*, 339.
(34) Stampfli, P. *Z. Phys. D* **1997**, *40*, 345−346.
(35) Haberland, H. *Surf. Sci.* **1985**, *156*, 305.
(36) Durand, G.; Amarouche, M.; Malrieu, J. P. *J. Chem. Phys.* **1988**, *88* (2), 1010.